19

Intrinsic Interface Coupling in Ferroelectric Heterostructures and Superlattices

K.-H. Chew[1], L.-H. Ong[2] and M. Iwata[3]
[1]Department of Physics, University of Malaya, 50603 Kuala Lumpur,
[2]School of Physics, Universiti Sains Malaysia, 11800 Minden, Penang,
[3]Department of Engineering Physics, Electronics and Mechanics,
Graduate School of Engineering, Nagoya Institute of Technology, Nagoya,
[1,2]Malaysia
[3]Japan

1. Introduction

Ferroelectric superlattices comprising two or more different layers have received immense attention due to their potential applications, as well as their striking new or enhanced behaviors (Nakagawara et al., 2000; Dawber et al., 2005). In those structures, the coupling at the interface between the two constituents has been demonstrated to play an important role in governing their properties (Bousquet et al., 2005). Theoretical study of interface coupling in ferroelectric superlattices was initially performed based on the Landau-like formulation by taking the continuum limit of the transverse Ising model (Qu et al., 1997). In their model, the extrapolation lengths describe the inhomogeneity of polarizations near the surfaces and an interface-related parameter gives the strength of the coupling at the interface. We have recently proposed a thermodynamic model with only one unknown parameter to study the effect of interface on polarization behaviours at the interface region between two bulk ferroelectrics (Chew et al., 2003; Tsang et al., 2004). The intrinsic ferroelectric coupling at the interface leads to variation of polarization across the interface of the heterostructures.

In this contribution, we discuss some fundamental properties of the physics of interfaces in ferroelectric heterostructures and superlattices using the Landau-Ginzburg theory. The key issue that will be addressed is how the intrinsic ferroelectric coupling at the interface affects the physical properties of the hybrid structures such as phase transitions, polarization modulation profiles and dielectric susceptibilities. We begin with a discussion for heterostructure of interfaces between a bulk ferroelectrics and dielectrics, in which the influence of thickness is not significant. Explicit expressions describe the spatial profile of polarization at the interface region of the heterostructure are obtained (Chew et al., 2003). The influence of the intrinsic interface coupling on the inhomogeneity and discontinuity or continuity of polarization at the interface is illustrated.

Since ferroelectric superlattice is an interesting system to study the interface effect, the influence of thickness on the polarization profiles of the superlattice is investigated. Analytical expressions of the polarization profile for superlattices are derived and discussed in detailed (Ishibashi et al., 2007; Chew et al., 2009). Explicit expressions for dielectric

susceptibilities in the paraelectric phase of the superlattice are also obtained (Chew et al., 2008). Finally, we apply the model to epitaxial $PbTiO_3/SrTiO_3$ by incorporating the depolarization field and lattice strain in the free energy functional. Some calculated results are discussed with experimental data. We conclude the chapter with some remarks.

2. Model of ferroelectric/dielectric heterostructure interfaces

In this section, the essential details for deriving the formalism of the ferroelectric/dielectric heterostructure interface are presented (Chew et al., 2003). We assume a one-dimensional problem in which the polarizations and related physical quantities vary along the *x*-direction perpendicular to the interface of the heterostructure. The total energy associates with the heterostructure can be expressed as

$$F = F_1 + F_2 + F_i, \tag{1}$$

where F_1 and F_2 are the total free energy density of the ferroelectric constituent *A* and dielectric constituent *B*, respectively. F_i is the coupling energy at the interface between the two constituents.

The total free energy density of the ferroelectric constituent *A* and dielectric constituent *B* are given by

$$\begin{cases} F_1 = \int \left(f_1 - f_1^{'} \right) dx, \\ F_2 = \int \left(f_2 - f_2^{'} \right) dx, \end{cases} \tag{2}$$

which extend from $x \to -\infty$ to $x = 0$ and $x = 0$ to $x \to \infty$, respectively. f_j denotes the Landau-Ginzburg free energy densities of consituent layer j, whereas $f_j^{'}$ gives the energy density in the single domain state of constituent *j*.

In the present study, the coupling energy F_i between the polarizations at the interface is described as

$$F_i = \frac{\lambda}{2}(p_i - q_i)^2, \tag{3}$$

where p_i and q_i are the interface polarizations at $x = 0$. λ is the coupling constant describing the strength of the interaction.

The free energy density of the ferroelectric constituent *A* with $p^2 = p_b^2 = -\alpha_1/\beta_1$ in the bulk $(x \to -\infty)$ is given by

$$f_1 - f_1^{'} = \frac{\alpha_1}{2}p^2 + \frac{\beta_1}{4}p^4 + \frac{\kappa_1}{2}\left(\frac{dp}{dx}\right)^2 - \left(\frac{\alpha_1}{2}p_b^2 + \frac{\beta_1}{4}p_b^4\right). \tag{4}$$

For the dielectric constituent *B*, we have $q = q_b = 0$ at $x \to \infty$, and the free energy density contribution from the dielectric constituent (with the higher order $\beta_2 q^4 / 4$ term truncated) is

$$f_2 - f_2^{'} = \frac{\alpha_2}{2}q^2 + \frac{\kappa_2}{2}\left(\frac{dq}{dx}\right)^2, \tag{5}$$

because $f_2^{'} = 0$ for a non-polar dielectric. p and q are the order parameters of the ferroelectric and dielectric consituents, respectively. α_1 is a temperature-dependent parameter

$$\alpha_1 = \alpha_{10}(T - T_0), \tag{6}$$

where $\alpha_{10} > 0$ is a temperarature-independent parameter. $\alpha_2 > 0$, $\beta_1 > 0$, $\kappa_1 > 0$ and $\kappa_1 > 0$ are all temperature-independent coefficients.

The equilibrium states of the heterostructures correspond to the minima of F with respect to variations of p and q. These are given by solving the Euler-Lagrange equations for p and q:

$$\begin{cases} \dfrac{\partial F}{\partial p} - \dfrac{\partial}{\partial x}\left(\dfrac{\partial F}{\partial p'}\right) = 0, \\ \dfrac{\partial F}{\partial q} - \dfrac{\partial}{\partial x}\left(\dfrac{\partial F}{\partial q'}\right) = 0, \end{cases} \tag{7}$$

with the boundary conditions

$$\begin{cases} p = p_i \\ q = q_i \end{cases} \text{ at } x = 0, \tag{8a}$$

and

$$\begin{cases} p = p_b \text{ and } \dfrac{dp}{dx} = 0 \quad \text{at } x \to -\infty, \\ q = q_b \text{ and } \dfrac{dq}{dx} = 0 \quad \text{at } x \to +\infty, \end{cases} \tag{8b}$$

where p_b and q_b are the bulk polarization of the ferroelectric constituent A (at x = -∞) and the dielectric constituent B (at $x = \infty$), respectively.

For the present study of ferroelectric/dielectric heterostructure of interface, it turns out that the free energy F of eq. (1) can be rewritten in terms of the interface polarizations p_i and q_i as order parameters. This gives F as a function of p_i and q_i without the usual integral form. Solving eqs. (1) and (7) simultaneously with the boundary conditions (i.e. eqs. (8a) and (8b)) imposed, and integrating once, the Euler-Lagrange equations becomes,

$$\frac{\alpha_1}{2}(p^2 - p_b^2) + \frac{\beta_1}{4}(p^2 - p_b^4) = \frac{\kappa_1}{2}\left(\frac{dp}{dx}\right)^2, \tag{9}$$

and

$$\frac{\alpha_2}{2}q^2 = \frac{\kappa_2}{2}\left(\frac{dq}{dx}\right)^2. \tag{10}$$

By solving eq. (9), the polarization of the ferroelectric constituent A becomes

$$p = p_b \tanh \frac{K_1}{\sqrt{2}}(x_i - x), \tag{11}$$

where

$$K_1 = \sqrt{-\frac{\alpha_1}{\kappa_1}}. \tag{12}$$

For the dielectric constituent *B*, the solution of eq. (10) gives

$$q = q_i \exp(-K_2 x), \tag{13}$$

with

$$K_2 = \sqrt{\frac{\alpha_2}{\kappa_2}}. \tag{14}$$

If p_i is determined, x_i can be obtained from eq. (11). In eqs. (11) and (13), the magnitude of the interface polarizations p_i and q_i are determined by the interface coupling parameter λ. The total energy, eq. (1), of the heterostructure can be written in terms of p_i and q_i as

$$F = \frac{1}{3}\sqrt{\frac{\beta_1 \kappa_1}{2}}(p_i^3 - 3p_i p_b^2 + 2p_b^3) + \frac{\sqrt{\alpha_2 \kappa_2}}{2} q_i^2 + \frac{\lambda}{2}(p_i - q_i)^2. \tag{15}$$

The equilibrium structure can be found from

$$\frac{\partial F}{\partial p_i} = \sqrt{\frac{\beta_1 \kappa_1}{2}}(p_i^2 - p_b^2) + \lambda(p_i - q_i) = 0, \tag{16}$$

and

$$\frac{\partial F}{\partial q_i} = \sqrt{\alpha_2 \kappa_2} q_i - \lambda(p_i - q_i) = 0. \tag{17}$$

Let us examine the variation of polarization across the interface and the total energy F of the heterostructure for the particular conditions of $\lambda = 0$ and $\lambda \to \infty$. The variation of polarization across the interface can be examined by looking into the continuity or discontinuity in interface polarizations $p_i - q_i$. Without interface coupling ($\lambda = 0$), we find that $p_i = p_b$ and $q_i = 0$. Thus, the mismatch of interface polarizations and the total energy of the heterostructure are found to be

$$p_i - q_i = p_b, \tag{18}$$

and

$$F = 0, \tag{19}$$

respectively.

For a strong interface coupling, i.e., $\lambda \to \infty$, we have $p_i = q_i$, implying that the polarization is continuos across the interface. In order to find $p_i = q_i$, it is convenient to write eq. (15) in term of only p_i as

$$F = \frac{1}{3}\sqrt{\frac{\beta_1 \kappa_1}{2}}(p_i^3 - 3p_i p_b^2 + 2p_b^3) + \frac{\sqrt{\alpha_2 \kappa_2}}{2} p_i^2 , \tag{20}$$

and by minimizing it, we obtain

$$p_i = q_i = p_b \left\{ \sqrt{1 + \frac{1}{2}\left(-\frac{\alpha_2}{\alpha_1}\right)\left(\frac{\kappa_2}{\kappa_1}\right)} - \sqrt{\frac{1}{2}\left(-\frac{\alpha_2}{\alpha_1}\right)\left(\frac{\kappa_2}{\kappa_1}\right)} \right\}, \tag{21}$$

which clearly indicates that the polarizations at the interface are determined by the intermixed properties of two constituents.

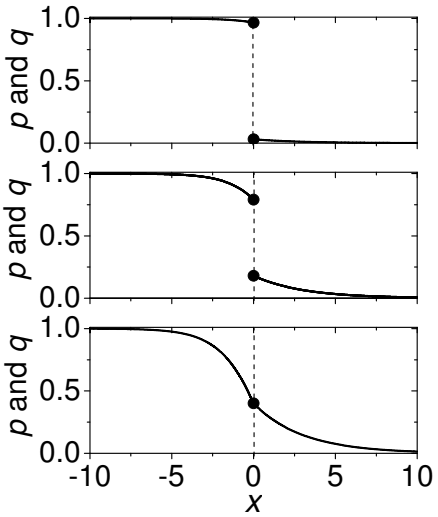

Fig. 1. Spatial dependence of polarization at the interface region of ferroelectric/dielectric heterostructures with $\lambda^{-1} = 10$ (top), 1 (middle) and 0 (bottom). In the curves, the parameters are: $\alpha_1 = -1$, $\alpha_2 = 1$, $\beta_1 = 1$, $\kappa_1 = 4$ and $\kappa_2 = 9$. Solid circles denote the polarization at interface.

Figure 1 shows a typical example of a ferroelectric/dielectric heterostrucutre of interface with different strength of interface coupling λ. It is seen that the mismatch in the polarization across the interface is notable for a loose coupling at the interface $\lambda^{-1} = 10$. The mismatch in the interface polarization becomes smaller with increasing coupling strength. It is interesting to see that the coupling at the interface induces polarization in the dielectric consituent. This may be called the interface-induced polarization, and it extends into the bulk over a distance governed by the characteristic length of the material K_2^{-1}, which is governed by α_2 and κ_2.

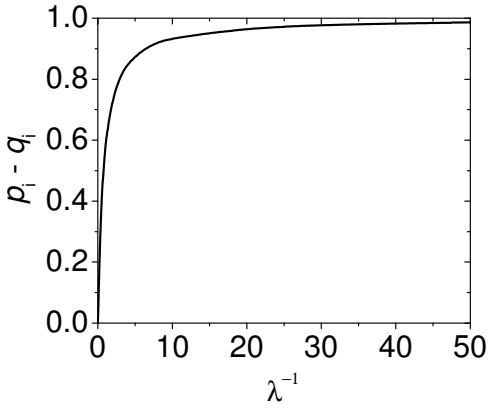

Fig. 2. Mismatch in the polarization at the interface of ferroelectric/dielectric heterostructures as a function of λ^{-1}. Other parameters are the same as for Fig. 1.

In Fig. 2, the mismatch in polarizations across the interface is examined under various strengths of interfacial coupling. The results clearly show that the mismatch in the interface polarizations is decreased with increasing interface coupling strength.

3. Model of ferroelectric/dielectric superlattices

We now consider a periodic superlattice composed of alternating ferroelectric layer and dielectric layer (ferroelectric/dielectic suprelattices), as shown in Fig. 3. Some key points are repeated here for clarity of discussion. Similarly, we assume that all spatial variation of polarization takes place along the x-direction. The thickness of ferroelectric layer and dielectric layer are L_1 and L_2, respectively. L is the periodic thickness of the superlattice. The two layers are coupled with each other across the interface. Periodic boudary conditions are used for describing the superlattices.

By symmetry, the average energy density of the ferroelectric/dielectric superlattice F is (Ishibashi & Iwata, 2007; Chew et al., 2008; Chew et al., 2009)

$$F = \frac{2}{L}\left(F_1 + F_2 + F_i\right). \tag{22}$$

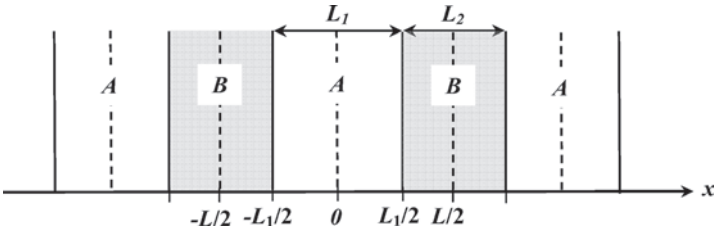

Fig. 3. Schematic illustration of a periodic ferroelectric superlattice composed of a ferroelectric and dielectric layers. The thickness of ferroelectric layer A and dielectric layer B are L_1 and L_2, respectively. $L = L_1 + L_2$ is the periodic thickness of the superlattice.

In eq. (22), the total free energy density of the ferroelectric layer F_1 is given by

$$F_1 = \int_0^{L_1/2} \left(\frac{\alpha_1}{2} p^2 + \frac{\beta_1}{4} p^4 + \frac{\kappa_1}{2} \left(\frac{\mathrm{d}p}{\mathrm{d}x} \right)^2 - pE \right) dx \,, \tag{23}$$

whereas the total free energy densities of the paraelectric layer f_2 is

$$F_2 = \int_{L_1/2}^{L/2} \left[\frac{\alpha_2}{2} q^2 + \frac{\kappa_2}{2} \left(\frac{\mathrm{d}q}{\mathrm{d}x} \right)^2 - qE \right] \mathrm{d}x \,, \tag{24}$$

respectively. In eqs. (23) and (24), p and q are the order parameters of the ferroelectric layer and paraelectric layer, respectively. E denotes the external electric field.
The coupling energy at the interface between the ferroelectric- and dielectric-layers is as shown in eq. (3). In this case, the boundary conditions at the interface (x = $L_1/2$) are described by

$$\begin{cases} \dfrac{\mathrm{d}p}{\mathrm{d}x} = -\dfrac{\lambda}{\kappa_1} (p_\mathrm{i} - q_\mathrm{i}) \,, \\ \dfrac{\mathrm{d}q}{\mathrm{d}x} = \dfrac{\lambda}{\kappa_2} (p_\mathrm{i} - q_\mathrm{i}) \,. \end{cases} \tag{25}$$

3.1 Polarization modulation profiles

We first look at the polarization modulation profiles of the ferroelectric/dielectric superlattice under the absence of an external electric field $E = 0$ (Chew et al., 2009). The polarization profiles of p and q for the ferroelectric and dielectric layers, respectively, can be obtained using the Euler-Lagrange equation. For the dielectric layer, the Euler-Lagrange equation is

$$\kappa_2 \frac{\mathrm{d}^2 q}{\mathrm{d}x^2} = \alpha_2 q \,, \tag{26}$$

and $q(x)$ can be obtained as

$$q(x) = q_\mathrm{c} \cosh K_2 \left(x - \frac{L}{2} \right) , \tag{27}$$

and at the interface, we have

$$q_i = q_\mathrm{c} \cosh \frac{K_2 L_2}{2} \,, \tag{28}$$

where q_c is the q value at $\mathrm{d}q / \mathrm{d}x = 0$.
By integrating once, the Euler-Lagrange equation of the ferroelectric layer is

$$\frac{\kappa_1}{2} \left(\frac{\mathrm{d}p}{\mathrm{d}x} \right)^2 = \frac{\alpha_1}{2} \left(p^2 - p_\mathrm{c}^2 \right) + \frac{\beta_1}{4} \left(p^4 - p_\mathrm{c}^4 \right) , \tag{29}$$

where p_c is the p value at $dp/dx = 0$. In this case, p_c is the maximum value of p at $x = 0$. Using $p(x) = p_c \sin\theta(x)$ and $p_b^2 = -\alpha_1/\beta_1$, eq. (29) becomes

$$\sqrt{\frac{-\alpha_1}{\kappa_1(1+k^2)}} \int_{-L_1/2}^{x} dx = \int_{\theta_i}^{\theta} \frac{d\theta}{\sqrt{1-k^2\sin^2\theta}}, \tag{30}$$

where $F(\theta,k)$ and $F(\theta_i,k)$ are the elliptic integral of the first kind with the elliptic modulus k given by

$$k^2 = \frac{p_c^2}{2p_b^2 - p_c^2}. \tag{31}$$

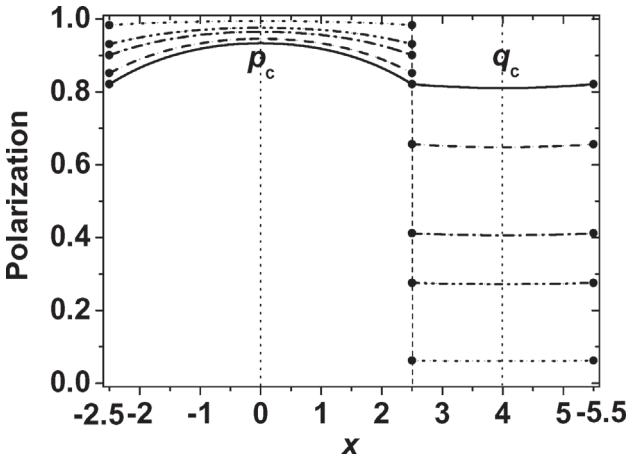

Fig. 4. Spatial dependence of polarization for a superlattice with $L_1 = 5$ and $L_2 = 3$ for various λ^{-1}. The parameters adopted for the calculation are: $\alpha_1 = -1$, $\alpha_2 = 0.1$, $\beta_1 = 1$, $\beta_2 = 1$, $\kappa_1 = 4$ and $\kappa_2 = 9$. In the curves, the values for λ^{-1} are: 100 (dot), 16 (dash-dot-dot), 8 (dash-dot), 2 (dash), and 0 (solid). Dotted circles represent the interface polarizations (Chew et al., 2009).

Let us discuss the polarization modulation profiles in a ferroelectric/dielectric superlattice using the explicit expressions. The characteristic lengths of polarization modulations in the ferroelectric layer near the transition point and the dielectric layer are given by $K_1^{-1} = \sqrt{-\kappa_1/\alpha_1}$ and $K_2^{-1} = \sqrt{\kappa_2/\alpha_2}$, respectively. Figure 4 illustrates an example of λ^{-1} dependence of polarization modulation profiles. It is seen that the modulation of the polarization is obvious in the ferroelectric layer, but not in the dielectric layer. This is because $L_1/2 > \sqrt{-\kappa_1/\alpha_1} = 2$ and $L_2/2 < \sqrt{\kappa_2/\alpha_2} \approx 0.95$. For a loosely coupled superlattice of $\lambda^{-1} = 100$ (dot lines), only a weak polarization is induced in the dielectric layer. As the strength of the interface coupling λ increases, the polarization near the interface of the ferroelectric layer is slightly suppressed, whereas the induced-polarization of the soft dielectric layer increases.

3.2 Phase transitions

Using the explicit expressions (as obtained in Sect. 3.1), the average energy density of the superlattice F (eq. (22)) can be written in terms of p_c and q_c as (Chew et al., 2009)

$$F = \frac{2}{L}\left[\sqrt{\frac{-\alpha_1\kappa_1}{1+k^2}}Jp_c^2 + \left(\frac{\alpha_1}{2}p_c^2 + \frac{\beta_1}{4}p_c^4\right)\frac{L_1}{2} + \frac{\lambda}{2}p_c^2\sin^2\theta_i - Cp_cq_c + \frac{D}{2}q_c^2\right], \tag{32}$$

where

$$\begin{cases} C = \lambda\cosh\left(\dfrac{K_2L_2}{2}\right)\cdot\sin\theta_i, \\ D = \dfrac{\sqrt{\alpha_2\kappa_2}}{2}\sinh\left(K_2L_2\right) + \lambda\cosh^2\left(\dfrac{K_2L_2}{2}\right), \\ J = \int_{\pi/2}^{\theta_i}\cos^2\theta\sqrt{1-k^2\sin^2\theta}\;d\theta, \end{cases} \tag{33}$$

with $\theta_i = \sin^{-1}\left(p_i / p_c\right)$. By utilizing $k^2 \approx p_c^2 / \left(2p_b^2\right)$ and K_1 (see eq. (12)) near the transition point, F becomes

$$F = \frac{2}{L}\left[\frac{A}{2}p_c^2 + O\left(p_c^4\right) - Cp_cq_c + \frac{D}{2}q_c^2\right], \tag{34}$$

where

$$A = -\frac{\sqrt{-\alpha_1\kappa_1}}{2}\sin K_1L_1 + \lambda\cos^2\frac{K_1L_1}{2}\ , \tag{35}$$

and $O(p_c^4)$ indicates the higher order terms of p_c^4.

From the equilibrium condition for q_c, $\mathrm{d}F/\mathrm{d}q_c = 0$, the condition of the transition point can be obtained as $A - C^2/D = 0$, i.e.,

$$-\frac{\sqrt{-\alpha_1\kappa_1}}{2}\sin K_1L_1 + R\cos^2\frac{K_1L_1}{2} = 0\,, \tag{36}$$

where

$$R = \frac{\lambda r}{\lambda + r}, \quad r = \sqrt{\alpha_2\kappa_2}\tanh\frac{K_2L_2}{2}\,. \tag{37}$$

In Fig. 5, we show the dependence of p_c and q_c on λ^{-1} for different dielectric stiffness α_2. For a superlattice with a soft dielectric layer $\alpha_2 = 0.1$ and 1, p_c remains almost the same as the bulk polarization $p_c \sim p_b$ for all λ^{-1}. For the case with $\alpha_2 = 5$, p_c is suppressed near the strong coupling regime $\lambda^{-1} \sim 0$. If the dielectric layer is very rigid (α_2 = 10 and 50), we found that p_c is strongly suppressed with increasing interface coupling and q_c remains very weak. It is seen that the polarizations of the superlattices with rigid dielectric layers are completely disappeared at $\lambda^{-1} \approx$ 0.0514 and 0.1189, respectively. These transition points can be obtained using eq. (36).

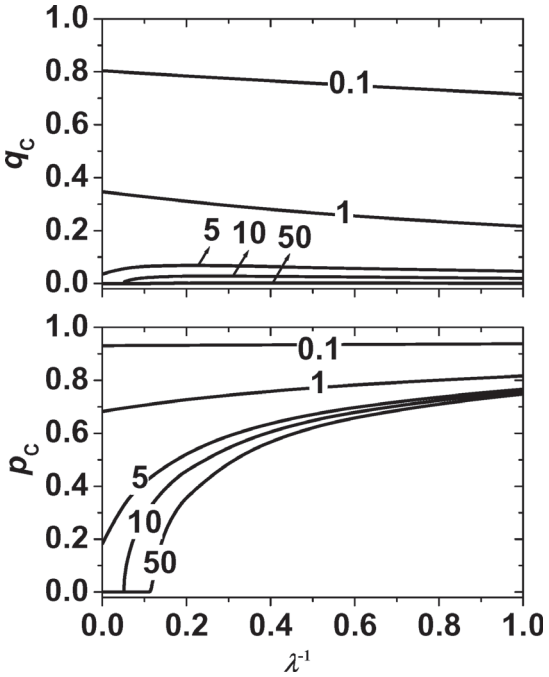

Fig. 5. p_c and q_c as a function of λ^{-1} for various α_2, where α_2 is 0.1, 1, 5, 10, and 50. The other parameters are the same as Fig. 4 (Chew et al., 2009).

As the temperature increases, the ferroelectric layer can be in the ferroelectric state or in the paraelectric state. Phase transition may or may not take place, depending on the model parameters. Let us examine the stability of superlattice in the paraelectric state by taking into account the polarization profile to appear in the ferroelectric state. Instead of the exact solutions obtained from the Euler-Lagrange equations, which are in term of the Jacobi Elliptic Functions, we use (Ishibashi & Iwata, 2007)

$$p = p_c \cos K_1 x \,, \tag{38}$$

thus p_i becomes

$$p_i = p_c \cos \frac{K_1 L_1}{2} \,. \tag{39}$$

The Euler-Lagrange equation for q is given by eq. (26), which gives $q(x)$ as expressed in eq. (27). Substitution of eqs. (27) and (38) into eq. (22), F becomes

$$F = \frac{2}{L}\left[\frac{a_1}{2} p_c^2 + \frac{b_1}{4} p_c^4 + \frac{a_2}{2} q_c^2 - c p_c q_c \right], \tag{40}$$

where

$$\begin{cases} a_1 = \dfrac{1}{4}\left[\left(\alpha_1 + \kappa_1 K_1^2\right)L_1 + \dfrac{\alpha_1 - \kappa_1 K_1^2}{K_1}\sin K_1 L_1\right] + \lambda\cos^2\left(\dfrac{K_1 L_1}{2}\right), \\ b_1 = \dfrac{\beta_1}{4}\left(\dfrac{3L_1}{4} + \dfrac{\sin K_1 L_1}{K_1} + \dfrac{\sin 2K_1 L_1}{8K_1}\right), \\ a_2 = \dfrac{\alpha_2}{K_2}\sinh\dfrac{K_2 L_2}{2}\cosh\dfrac{K_2 L_2}{2} + \lambda\cosh^2\dfrac{K_2 L_2}{2}, \\ c = \lambda\cos\dfrac{K_1 L_1}{2}\cosh\dfrac{K_2 L_2}{2}. \end{cases} \tag{41}$$

Similarly, from the equilibrium condition for q_c, $dF/dq_c = 0$, we find eq. (40) can be reduced to a more simple form as

$$F = \frac{2}{L}\left[\frac{a_1^*}{2}p_c^2 + \frac{b_1}{4}p_c^4\right], \tag{42}$$

where

$$a_1^* = \frac{L_1}{4}\left[\alpha_1 + \kappa_1 K_1^2 + \frac{\alpha_1 - \kappa_1 K_1^2}{K_1 L_1}\sin K_1 L_1\right] + R\cos^2\frac{K_1 L_1}{2}, \tag{43}$$

where $R(\lambda, r)$ is given by eq. (37). r is a function of α_2, κ_2 and L_2. The transitions of the superlattice from a paraelectric phase to a ferroelectric state occurs when $a_1^* = 0$. Note here that a_1^* consists of the physical parameters from both the ferroelectric and dielectric layers. It is seen that the influence of the dielectric layer via λ becomes stronger with increasing α_2, κ_2 and L_2. However, the influence is limited at most to $r_{\max} = \sqrt{\alpha_2 \kappa_2}$. Let us look at a_1^* in more detail. By taking $\left.\dfrac{\partial a_1^*}{\partial K_1}\right|_{K_1 = k} = 0$, we obtain the wave number k. It is qualitatively

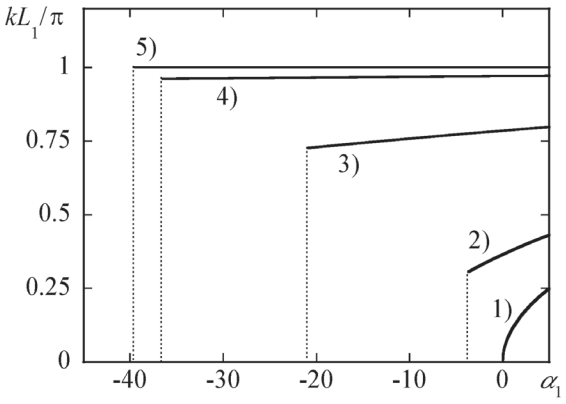

Fig. 6. The dependence of the wave number k for various R/L_1 when $\kappa_1 = 1$ and $L_1 = 1/2$. The curves show the cases 1) $R/L_1 = 0$, 2) $R/L_1 = 2$, 3) $R/L_1 = 20$, 4) $R/L_1 = 200$ and 5) $R/L_1 = \infty$. Dotted lines denote the transition point of each case (Ishibashi & Iwata, 2007).

obvious that k is small, implying a flat polarization profile, when the contribution from the dielectric layer R, is small, while kL_2 approaches π, implying a very weak interface polarization in the ferroelectric layer, when R is extremely large. The dependence of the wave number k on α_1 for various R / L_1 is illustrated in Fig. 6.

3.3 Dielectric susceptibilities

In this section, we will discuss the dielectric susceptibility of the superlattice in the paraelectric phase (Chew et al., 2008). Since $p(x) = q(x) = 0$ in the paraelectric phase (if $E = 0$), the modulated polarizations, $p(x)$ and $q(x)$, are the polarizations induced by the electric field E. The contribution from the higher-order term $\beta_1 p^4 / 4$ is neglected because we consider only the paraelectric phase. By solving the Euler-Lagrange equations, we found

$$\begin{cases} \alpha_1 p - \kappa_1 \dfrac{\mathrm{d}^2 p}{\mathrm{d}x^2} = E, \\ \alpha_2 q - \kappa_2 \dfrac{\mathrm{d}^2 q}{\mathrm{d}x^2} = E, \end{cases} \tag{44}$$

with the condition that F (eq. (22)) including the interface energy (eq. (3)) takes the minimum value. Note that in the present system, the ferroelectric transition point α_c is negative. Thus, one must consider both cases $\alpha_1 \geq 0$ and $\alpha_1 < 0$ in the study of the dielectric susceptibility even in the paraelectric phase. In the present system, the dielectric susceptibility χ is defined as

$$\chi = \frac{2}{LE}\left[\int_0^{L_1/2} p\,\mathrm{d}x + \int_{L_1/2}^{L/2} q\,\mathrm{d}x\right]. \tag{45}$$

3.3.1 Case $\alpha_1 \geq 0$

For the case of $\alpha_1 \geq 0$, the exact solutions are

$$\begin{cases} p = p_{\mathrm{c}} E \cosh K_1 x + \dfrac{E}{\alpha_1}, \\ q = q_{\mathrm{c}} E \cosh K_2 \left(x - \dfrac{L}{2} \right) + \dfrac{E}{\alpha_2}, \end{cases} \tag{46}$$

and

$$\begin{cases} p_{\mathrm{i}} = p_{\mathrm{c}} E \cosh \dfrac{K_1 L_1}{2} + \dfrac{E}{\alpha_1}, \\ q_{\mathrm{i}} = q_{\mathrm{c}} E \cosh \dfrac{K_2 L_2}{2} + \dfrac{E}{\alpha_2}. \end{cases} \tag{47}$$

In this case, $K_1 = \sqrt{\alpha_1 / \kappa_1}$ and K_2 is given by eq. (14). By utilizing eqs. (46) and (47), we can express F in terms of p_c and q_c as

$$F = \frac{2}{L}\left(\frac{a_1}{2}p_c^2 + \frac{a_2}{2}q_c^2 - cp_cq_c - d_1p_c - d_2q_c\right)E^2, \tag{48}$$

where

$$\begin{cases} a_1 = \dfrac{\alpha_1}{2K_1}\sinh K_1L_1 + \lambda\cosh^2\dfrac{K_1L_1}{2}, \\ a_2 = \dfrac{\alpha_2}{2K_2}\sinh K_2L_2 + \lambda\cosh^2\dfrac{K_2L2}{2}, \\ c = \lambda\cosh\dfrac{K_1L_1}{2}\cosh\dfrac{K_2L_2}{2}, \\ d_1 = -\lambda\cosh\dfrac{K_1L_1}{2}\left(\dfrac{1}{\alpha_1} - \dfrac{1}{\alpha_2}\right), \\ d_2 = \lambda\cosh\dfrac{K_2L_2}{2}\left(\dfrac{1}{\alpha_1} - \dfrac{1}{\alpha_2}\right). \end{cases} \tag{49}$$

Using the equilibrium conditions $\partial F / \partial p_c = \partial F / \partial q_c = 0$, we find

$$p_c = \frac{-\lambda}{a_2A}\left(\frac{\alpha_2}{2K_2}\cosh\frac{K_1L_1}{2}\sinh K_2L_2\right)\left(\frac{1}{\alpha_1} - \frac{1}{\alpha_2}\right), \tag{50}$$

and

$$q_c = \frac{\lambda}{a_2A}\left(\frac{\alpha_1}{2K_1}\cosh\frac{K_2L_2}{2}\sinh K_1L_1\right)\left(\frac{1}{\alpha_1} - \frac{1}{\alpha_2}\right), \tag{51}$$

where

$$A = a_1 - \frac{c^2}{a_2}. \tag{52}$$

Based on eq. (45), the dielectric susceptibility for the present case is

$$\chi = \frac{2p_c}{K_1L}\sinh\frac{K_1L_1}{2} + \frac{L_1}{L\alpha_1} + \frac{2q_c}{K_2L}\sinh\frac{K_2L_2}{2} + \frac{L_2}{L\alpha_2}. \tag{53}$$

3.3.2 Case $\alpha_1 < 0$

In this case, the exact solutions of eq. (44) are

$$\begin{cases} p = p_cE\cos K_1x + \dfrac{E}{\alpha_1}, \\ q = q_cE\cosh K_2\left(x - \dfrac{L}{2}\right) + \dfrac{E}{\alpha_2}, \end{cases} \tag{54}$$

where K_1 and K_2 are given by eq. (12) and (14), respectively. Thus, we have

$$\begin{cases} p_{\mathrm{i}} = p_{\mathrm{c}} E \cos\dfrac{K_1 L_1}{2} + \dfrac{E}{\alpha_1}, \\ q_{\mathrm{i}} = q_{\mathrm{c}} E \cosh\dfrac{K_2 L_2}{2} + \dfrac{E}{\alpha_2}. \end{cases} \tag{55}$$

Similarly, we find

$$F = \frac{2}{L}\left(\frac{a_1}{2} p_{\mathrm{c}}^2 + \frac{a_2}{2} q_{\mathrm{c}}^2 - c p_{\mathrm{c}} q_{\mathrm{c}} - d_1 p_{\mathrm{c}} - d_2 q_{\mathrm{c}} \right) E^2 , \tag{56}$$

where

$$\begin{aligned} a_1 &= \frac{\alpha_1}{2K_1}\sin K_1 L_1 + \lambda \cos^2\frac{K_1 L_1}{2}, \\ a_2 &= \frac{\alpha_2}{2K_2}\sinh K_2 L_2 + \lambda \cosh^2\frac{K_2 L_2}{2}, \\ c &= \lambda \cos\frac{K_1 L_1}{2}\cosh\frac{K_2 L_2}{2}, \\ d_1 &= -\lambda \cos\frac{K_1 L_1}{2}\left(\frac{1}{\alpha_1} - \frac{1}{\alpha_2} \right), \\ d_2 &= \lambda \cosh\frac{K_2 L_2}{2}\left(\frac{1}{\alpha_1} - \frac{1}{\alpha_2} \right), \end{aligned} \tag{57}$$

and the the values of p_{c} and q_{c} become

$$p_{\mathrm{c}} = \frac{-\lambda}{a_2 A}\left(\frac{\alpha_2}{2K_2}\cos\frac{K_1 L_1}{2}\sinh K_2 L_2 \right)\left(\frac{1}{\alpha_1} - \frac{1}{\alpha_2} \right), \tag{58}$$

and

$$q_{\mathrm{c}} = \frac{\lambda}{a_2 A}\left(\frac{\alpha_1}{2K_1}\cosh\frac{K_2 L_2}{2}\sin K_1 L_1 \right)\left(\frac{1}{\alpha_1} - \frac{1}{\alpha_2} \right), \tag{59}$$

with

$$A = a_1 - \frac{c^2}{a_2}. \tag{60}$$

Using eqs. (45), the dielectric susceptibility χ for the present case of $\alpha_1 < 0$ is

$$\chi = \frac{2p_{\mathrm{c}}}{K_1 L}\sin\frac{K_1 L_1}{2} + \frac{L_1}{L\alpha_1} + \frac{2q_{\mathrm{c}}}{K_2 L}\sinh\frac{K_2 L_2}{2} + \frac{L_2}{L\alpha_2}, \tag{61}$$

where the phase transition point is given by $A = a_1 - c^2 / a_2 = 0$. Using $A = a_1 - c^2 / a_2 = 0$, the condition of the transition point is

$$\frac{\alpha_1}{2K_1}\sin K_1 L_1 + \frac{\lambda\frac{\alpha_2}{2K_2}\sin K_2 L_2}{\frac{\alpha_2}{2K_2}\sin K_2 L_2 + \lambda\cosh^2\frac{K_2 L_2}{2}}\cos^2\frac{K_1 L_1}{2} = 0. \tag{62}$$

It is interesting to note here that the transition temperature α_1 can be determined using eq. (62), which is exactly the same as eq. (43) (Ishibashi & Iwata, 2007).

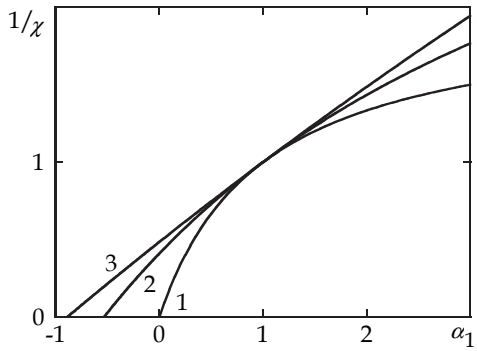

Fig. 7. Reciprocal susceptibility as a function of α_2. The parameter values are adopted as $L = 1$, $L_1 = L_2 = 1/2$, $\kappa_1 = \kappa_2 = 1$, $\alpha_2 = 1$, for cases of: (1) $\lambda = 0$, (2) $\lambda = 0.3$, (3) $\lambda = 3$ (Chew et al., 2008).

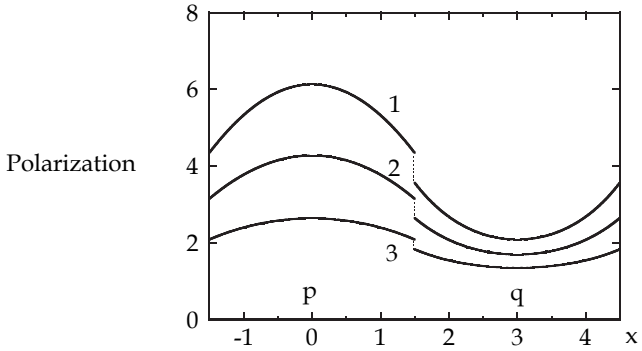

Fig. 8. Spatial dependence of polarization for a superlattice with $L_1 = L_2 = 3$. The parameters adopted for the calculation are: $\kappa_1 = \kappa_2 = 1$, $\alpha_2 = 1$, $\lambda = 3$, for cases of (1) $\alpha_1 = -0.1$, (2) $\alpha_1 = 0$, (3) $\alpha_1 = 0.2$ (Chew et al., 2008).

In Fig. 7, we show the reciprocal susceptibility $1/\chi$ in various parameter values. It is found that the average susceptibility diverges at the transition temperature obtained from eq. (62).

The result indicates that the second-order phase transition is possible in our model of the superlattice structure. It is seen that the susceptibility is continuous at $\alpha_1 = 0$, though the susceptibility is divided into two different functions at $\alpha_1 = 0$. Taking the limit of $\alpha_1 = \pm 0$ from both the positive and negative sides, the explicit expression for the susceptibility at $\alpha_1 = 0$ is

$$\chi = \frac{1}{2L}\left[\frac{2L_1 + L_2}{\alpha_2} + \frac{L_1^2}{2\lambda} + \frac{L_1^3}{12\kappa_1} + \frac{L_1^2 K_2}{\alpha_2}\frac{\cosh^2\frac{K_2 L_2}{2}}{\sinh K_2 L_2}\right], \tag{63}$$

implying that the susceptibility is always continuous at $\alpha_1 = 0$. It is worthwhile to look at the field-induced polarization profile at $\alpha_1 = 0$ because K_1 becomes zero at $\alpha_1 = 0$. By taking the limit of $\alpha_1 = \pm 0$ from both the positive and negative sides for the polarization p, the expressions for the polarization profiles in $p(x)$ and $q(x)$ can be explicitly expressed as

$$p(x) = \frac{E}{8\kappa_1}\left(L_1^2 - 4x^2\right) + \frac{EL_1}{2\lambda} + \frac{EK_2 L_1}{\alpha_2}\frac{\cosh^2\frac{K_2 L_2}{2}}{\sinh K_2 L_2} + \frac{E}{\alpha_2}, \tag{64}$$

and

$$q(x) = \frac{EK_2 L_1 \cosh\frac{K_2 L_2}{2}}{\alpha_2 \sinh K_2 L_2}\cosh\left[K_2\left(x - \frac{L}{2}\right)\right] + \frac{E}{\alpha_2} \tag{65}$$

Equation (64) depicts the polarization profile $p(x)$ that exhibits a parabolic modulation at $\alpha_1 = 0$, as shown in Fig. 8. The polarization profile obtained near the transition point may coincide with the polarization modulation pattern of the ferroelectric soft mode in the paraelectric phase.

3.4 Application of model to epitaxial $PbTiO_3/SrTiO_3$ superlattices

Let us extend the model to study the ferroelectric polarization of epitaxial $PbTiO_3/SrTiO_3$ (PT/ST) superlattices grown on ST substrate and under a short-circuit condition, as schematically shown in Fig. 9. Some key points from the previous sections are repeated here for clarity of discussion.

In this study, we need to include the effects of interface, depolarization field and substrate-induced strain in the model. By assuming that all spatial variation of polarization takes place along the z-direction, the Landau-Ginzburg free energy per unit area for one period of the PT/ST superlattice can be expressed as (Chew et al., *unpublished*)

$$F = F_{PT} + F_{ST} + F_I, \tag{66}$$

where the free energy per unit area for the PT layer with thickness L_{PT} is

$$F_{PT} = \int_{-L_{PT}}^{0}\left[\frac{\alpha_{PT}^*}{2}p^2 + \frac{\beta_{PT}^*}{4}p^4 + \frac{\gamma_{PT}}{6}p^6 + \frac{\kappa_{PT}}{2}\left(\frac{dp}{dz}\right)^2 + \frac{u_{m,PT}^2}{s_{11,PT} + s_{12,PT}} - \frac{1}{2}e_{d,PT}p\right]dz, \tag{67}$$

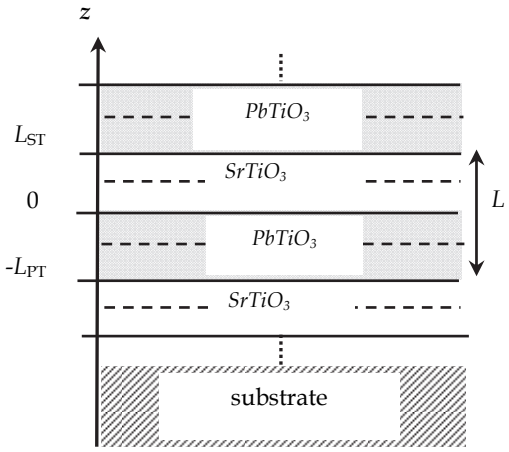

Fig. 9. Schematic illustration of a periodic superlattice composed of a ferroelectric and a paraelectric layers. The thicknesses of $PbTiO_3$ (PT) and $SrTiO_3$ (ST) layers are L_{PT} and L_{ST}, respectively. L denotes the periodic thickness of the PT/ST superlattice.

and the free energy per unit area for the ST layer with thickness L_{ST} is

$$F_{ST} = \int_0^{L_{ST}} \left[\frac{\alpha_{ST}^*}{2} q^2 + \frac{\beta_{ST}^*}{4} q^4 + \frac{\gamma_{ST}}{6} q^6 + \frac{\kappa_{ST}}{2} \left(\frac{dq}{dz} \right)^2 + \frac{u_{m,ST}^2}{s_{11,ST} + s_{12,ST}} - \frac{1}{2} e_{d,ST} q \right] dz. \tag{68}$$

where p and q corresponds to the polarization of PT and ST layers, respectively. For the superlattices with the polarizations perpendicular to the layer's surfaces/interfaces, the inhomogeneity of polarization means that the depolarization field effect is essential. In eqs. (67) and (68), α_j^* and β_j^* are expressed as

$$\left. \begin{aligned} \alpha_j^* &= \alpha_j - \frac{4Q_{12,j}}{s_{11,j} + s_{12,j}} u_{m,j}, \\ \beta_j^* &= \beta_j + \frac{4Q_{12,j}^2}{s_{11,j} + s_{12,j}}, \end{aligned} \right\} \tag{69}$$

where α_j, β_j and γ_j are the Landau coefficients of layer j (j : PT or ST), as usual. $s_{11,j}$ and $s_{12,j}$ are the elastic compliance coefficients, whereas $Q_{12,j}$ is the electrostrictive constant. $u_{m,j} = \left(a_S - a_j \right) / a_S$ denotes the in-plane misfit strain induced by the substrate due to the lattice mismatch. a_j is the unconstrained equivalent cubic cell lattice constants of layer j and a_S is the lattice parameter of the substrate. κ_j is the gradient coefficient, determining the energy cost due to the inhomogeneity of polarization.

With the assumption that the ferroelectric layers are insulators with no space charges, the depolarization field $e_{d,j}$ in the PT and ST layers can be expressed by

$$\begin{cases} e_{d,PT}(z) = -\dfrac{1}{\varepsilon_0}\big(p(z) - P\big), \\ e_{d,ST}(z) = -\dfrac{1}{\varepsilon_0}\big(q(z) - P\big), \end{cases} \tag{70}$$

respectively. In eq. (70), ε_0 denotes the dielectric permittivity in vacuum. The second term describes the mean polarization of one-period superlattice

$$P = \frac{1}{L}\left(\int_{-L_{PT}}^{0} p\,dz + \int_{0}^{L_{ST}} q\,dz \right), \tag{71}$$

with the periodic thickness $L = L_{PT} + L_{ST}$. It is important to note here that $e_{d,j}$ acts as the depolarization field, if its direction is opposite to the direction of ferroelectric polarization. If $e_{d,j}$ inclines in the same direction of polarization, it cannot be regarded as the depolarization field; thus, we denote $e_{d,j}$ as "the internal electric field". Hence, the average internal electric field of one-period superlattice is defined as

$$E_d = \frac{1}{L}\left[\int_{-L_{PT}}^{0} e_{d,PT}(z)dz + \int_{0}^{L_{ST}} e_{d,ST}(z)dz \right]. \tag{72}$$

The intrinsic coupling energy between the polarizations at the interfaces $z = 0$ of the two layers is described as

$$F_I = \frac{\lambda}{2}(p_i - q_i)^2, \tag{73}$$

where p_i and q_i are the interface polarizations at $z = 0$ for the PT and ST layers, respectively. In eq. (73), the parameter λ describes the strength of intrinsic interface coupling and it can be conveniently related to the dielectric permittivity in vacuum ε_0 as

$$\lambda = \frac{\lambda_0}{\varepsilon_0}, \tag{74}$$

where λ_0 denote the temperature-independent interface coupling constant. In this case, the existence of the interface coupling $\lambda \neq 0$ leads to the inhomogeneity of polarization near the interfaces, besides the effect of the depolarization field.

In the calculations, it is assumed that 1 *unit cell* (*u.c.*) ≈ 0.4 *nm* and the thickness of ST layer is maintained at $L_{ST} \approx 3$ *u.c.* The lattice constants in the paraelectric state are a_A = 3.969 Å and a_B = 3.905 Å for PT and ST layers, respectively. Based on the lattice constants, the lattice strains are obtained as $u_{m,PT}$ = −0.0164 and $u_{m,ST}$ = 0.

In Fig. 10, we show the average polarization P and internal electric fields E_d of PT/ST superlattices as a function of thickness ratio L_{PT}/L_{ST} for different strength of interface coupling λ_0. It is seen that P and E_d decrease with increasing λ_0. As λ_0 increases, the

critical thickness ratio (at which P vanishes) shifts to a higher value. It is seen that there is a good agreement between the calculated and measured polarizations. The calculated polarizations using $\lambda_0 = 10$ (black line) agree reasonably well with most of the experimental measurements for $L_{PT}/L_{ST} > 0.4$, implying that the strength of interface coupling at this regime is strong. At the $L_{PT}/L_{ST} \leq 0.4$ region, the predicted polarizations with $\lambda_0 = 0.2$ (red line) and 0.05 (blue line) agree well with some of the experimental measurements. The E_d versus L_{PT}/L_{ST} curves show a trend similar to P versus L_{PT}/L_{ST}, e.g. E_d disappears at a critical thickness ratio. For each λ_0, the critical thickness ratio of E_d coincides with that of P. It is remarkable to see that for $E_d > 0$, internal electric field is parallel to the direction of the ferroelectric polarization in PT layer, which enhances the polarization of the superlattice.

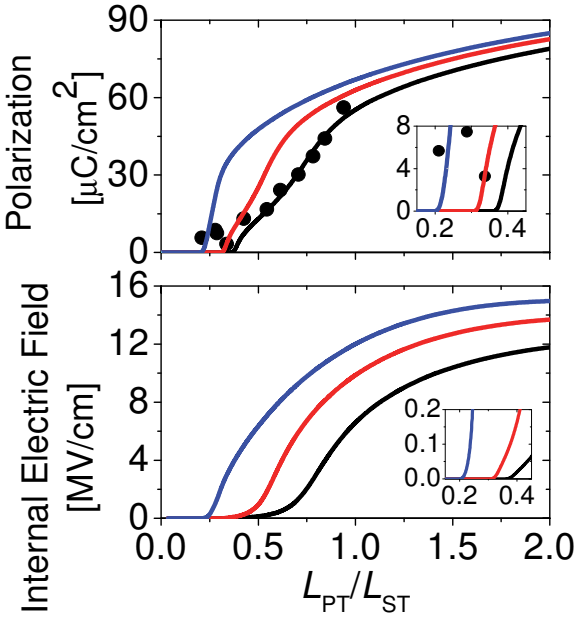

Fig. 10. Polarization and internal electric field as a function of thickness ratio L_{PT}/L_{ST} of PT/ST superlattices at T = 300K. The values of λ_0 are: 10 (—), 0.2 (—) and 0.05 (—). Solid dots (•) represent experimental results from Dawber et al (Dawber et al., 2007). The insets in each figure show the corresponding curves in smaller scale (Chew et al., *unpublished*).

4. Conclusion

We have proposed a model to study the intrinsic interface coupling in ferroelectric heterostructure and superlattices. The layered structure is described using the Landau-Ginzburg theory by incorporating the effect of coupling at the interface between the two constituents. Explicit analytical expressions describing the polarization at the interface

between bulk ferroelectrics and bulk dielectrics were derived and discussed. Here, we mainly discussed only cases where the transition of the ferroelectric constituent is of second order (Chew et al., 2003), though cases of heterostructure at the interfaces involving first-order phase transition were also reported (Tsang et al., 2004).

We further extend the model to investigate the ferroelectricity of superlattice by incorporating the thickness effect. Using the explicit expressions derived from the model, the polarization modulation profiles, phase transitions and dielectric susceptibilities of a superlattice are presented and discussed in detail (Ishibashi & Iwata, 2007; Chew et al., 2008; Chew et al., 2009). The effort to obtain the explicit analytical solutions using the continuum model of Landau-Ginzburg theory is worthwhile. This is because those expressions allow us to gain general insight on how the intrinsic polarization coupling at the interface influences the physical properties of those hybrid structures. Note that the effect of an applied electric field on the polarization behaviors of heterostructure at the interfaces (Chew et al., 2005; Chew et al., 2006) and superlattices (Chew et al., 2011; Chew et al., *unpublished*) is also very important. However, those studies were not discussed. We have also constructed a one-dimensional model on the basis of the Landau-Ginzburg theory to investigate the polarization and dielectric behaviors (Chew et al., 2006; Chew et al., 2007), as well as the switching characteristics (Chew et al., *unpublished*).

At the end of the discussion, we show how the present model can be applied to study the ferroelectric polarization of epitaxial PT/ST superlattices with the polarizations perpendicular to the surfaces/interfaces of the constituent layers (Chew et al., *unpublished*). The effects of interface, depolarization field and substrate-induced strain are required to include in the model. Our calculated polarizations (Chew et al., *unpublished*) agree reasonably well with recent experimental measurements (Dawber et al., 2007). From our study, it suggests that the recent experimental observation on the unusual recovery of ferroelectricity at thickness ratio of $L_{PT}/L_{ST} < 0.5$ (Dawber et al., 2005) may be related to a weakening of ferroelectric coupling at the interface. It is certainly interesting to look at the dielectric susceptibilities and polarization reversals of the superlattices, which will be reported elsewhere.

5. Acknowlegement

This work is supported by the University of Malaya Research Grant (No: RG170-11AFR). L. H. Ong acknowledges the support from FRGS Grant (No: 203/PFIZIK/6711144) by the Ministry of Higher Education, Malaysia.

6. References

Nakagawara, O.; Shimuta, T.; Makino, T.; Arai, S.; Tabata, H. & Kawai, T. (2000). Epitaxial Growth and Dielectric Properties of (111) Oriented $BaTiO_3/SrTiO_3$ Superlattices by Pulsed-laser Deposition, Applied Physics Letter, Vol. 77, No. 20, (November 2000), pp. 3257-3259, ISSN 0003-6951

Dawber, M.; Lichtensteiger, C.; Cantoni, M.; Veithen, M.; Ghosez, P.; Johnston, K.; Rabe, K. M.; & Triscone, J. M. (2005). Unusual Behavior of the Ferroelectric Polarization in

$PbTiO_3/SrTiO_3$ Superlattices, *Physical Review Letters*, Vol. 95, No.17, (October 2005), pp. 177601, ISSN 0031-9007

Bousquet, E.; Dawber, M.; Stucki, N.; Lichtensteiger, C.; Hermet, P.; Gariglio, S.; Triscone, J. M. & Ghosez, P. (2008). Improper Ferroelectricity in Perovskite Oxide Artificial Superlattices, *Nature*, Vol. 452, No. 7188, (April 2008), pp. 732-U4, ISSN 0028 - 0836

Qu, B. D.; Zhong, W. L.; & Prince, R. H. (1997) Interfacial Coupling in Ferroelectric Superlattices, *Physical Review B*, Vol. 55, No. 17, (May 1997), pp. 11218-11224, ISSN 0163-1829

Chew, K.-H.; Ishibashi, Y. ; Shin F. G. & Chan, H. L. W. (2003). Theory of Interface Structure in Double-Layer Ferroelectrics, *Journal of the Physical Society of Japan*, Vol. 72, No.9, (September 2003), pp. 3158-3165, ISSN 0031-9015

Tsang, C. H.; Chew, K.-H.; Ishibashi, Y. & Shin F. G. (2004). Structure of Interfaces in Layered Ferroelectrics of First and/or Second Order Transition, *Journal of the Physical Society of Japan*, Vol. 73, No.11, (November 2004), pp. 3158-3165, ISSN 0031-9015

Ishibashi, Y. & Iwata, M. (2007). Landau-Ginzburg Theory of Phase Transition of Ferroelectric Superlattices, *Ferroelectrics*, Vol. 354, (2007), pp. 8-12, ISSN 0015 - 0193

Chew, K.-H.; Iwata, M.; Ishibashi, Y. & Shin F. G. (2009). Polarization Modulation Profiles in Ferroelectric Superlattices, *Ferroelectrics Letters Section*, Vol. 36, No.1-2, (2009), pp. 12-19, ISSN 0731-5171

Chew, K.-H.; Iwata, M.; & Shin F. G. & Ishibashi Y. (2008). Exact Expressions for Dielectric Susceptibilities in the Paraelectric Phase of Ferroelectric Superlattices Based on Ginzburg-Landau Theory, *Integrated Ferroelectrics*, Vol. 100, No.1, (2008), pp. 79-87, ISSN 1058-4587

Dawber, M.; Stucki, N.; Lichtensteiger C.; Gariglio, S.; Ghosez, P. & Triscone J. M. (2007). Tailoring the Properties of Artificially Layered Ferroelectric Superlattices, *Advanced Materials*, Vol. 19, No. 23, (December 2007), pp. 4153-4159, ISSN 0935-9648

Chew, K.-H.; Ong, L.-H. & Iwata, M. Interface-induced Sign Change of Local Internal Electric Field in Nanoscale Ferroelectric Superlattices, (*unpublished*)

Chew, K.-H.; Ishibashi Y. & Shin F. G. (2005). Ferroelectric Hysteresis Loops as the Manifestation of Interfacial-aided Polarization Reversals in Ferroelectric Heterostructures, *J. Phys. Soc. Jpn.* Vol. 74, No. 8, (August 2005), pp. 2338-2346, ISSN 0031-9015

Chew, K.-H.; Ishibashi Y. & Shin F. G. (2006). Intrinsic Ferroelectric Hysteresis Behaviors for Heterostructures, *Physica Status Solidi A–Applications and Materials Science*. Vol. 203, No. 9, (July 2006) pp. 2205-2208, ISSN 0031-8965

Chew, K.-H.; Ong, L.-H. & Iwata, M. (2011). Switching Dynamics in Ferroelectric Superlattices, *Current Applied Physics*, Vol. 11, No.3, (May 2011), pp. 755-761, ISSN 15671739

Chew, K.-H.; Ong, L.-H. & Iwata, M. Influence of Dielectric Stiffness, Interface and Layer Thickness on Hysteresis Loops of Ferroelectric Superlattices, (*unpublished*)

Chew, K.-H.; Ishibashi, Y. & Shin F. G. (2006). A Lattice Model for Ferroelectric Superlattices, *Journal of the Physical Society of Japan*, Vol. 75, No.6, (June 2006), pp. 064712, ISSN 0031-9015

Chew, K.-H.; Ishibashi, Y. & Shin F.G. (2007). Competition between the Thickness Effects of Each Constituent Layer in Ferroelectric Superlattices, *Ferroelectrics*, Vol. 357, No.6, (2007), pp. 697-701, ISSN 0015-0193

Chew, K.-H., Ong L.-H. & Iwata M. A One-Dimensional Lattice Model of Switching Characteristics in Ferroelectric Superlattices, (*unpublished*)

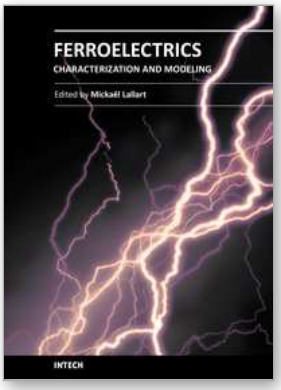

Ferroelectrics - Characterization and Modeling

Edited by Dr. MickaÃ«l Lallart

ISBN 978-953-307-455-9
Hard cover, 586 pages
Publisher InTech
Published online 23, August, 2011
Published in print edition August, 2011

Ferroelectric materials have been and still are widely used in many applications, that have moved from sonar towards breakthrough technologies such as memories or optical devices. This book is a part of a four volume collection (covering material aspects, physical effects, characterization and modeling, and applications) and focuses on the characterization of ferroelectric materials, including structural, electrical and multiphysic aspects, as well as innovative techniques for modeling and predicting the performance of these devices using phenomenological approaches and nonlinear methods. Hence, the aim of this book is to provide an up-to-date review of recent scientific findings and recent advances in the field of ferroelectric system characterization and modeling, allowing a deep understanding of ferroelectricity.

INTECH
open science | open minds

InTech Europe
University Campus STeP Ri
Slavka Krautzeka 83/A
51000 Rijeka, Croatia
Phone: +385 (51) 770 447
Fax: +385 (51) 686 166
www.intechopen.com

InTech China
Unit 405, Office Block, Hotel Equatorial Shanghai
No.65, Yan An Road (West), Shanghai, 200040, China
中国上海市延安西路65号上海国际贵都大饭店办公楼405单元
Phone: +86-21-62489820
Fax: +86-21-62489821